On the analytic solutions for squeezing flow of nanofluid between parallel disks

Meraj Mustafa Hashmi[a], **Tasawar Hayat**[b,c], **Ahmed Alsaedi**[c]

[a]Research Centre for Modeling and Simulation (RCMS)
National University of Sciences and Technology (NUST)
Islamabad 44000, Pakistan
meraj_mm@hotmail.com

[b]Department of Mathematics, Quaid-i-Azam University 45320
Islamabad 44000, Pakistan

[c]Department of Mathematics, Faculty of Science, King Abdulaziz University
P.O. Box 80257, Jeddah 21589, Saudi Arabia

Received: 13 March 2012 / **Revised:** 30 April 2012 / **Published online:** 22 November 2012

Abstract. This article investigates the magnetohydrodynamic squeezing flow of nanofluid between parallel disks. Governing partial differential equations are converted into ordinary differential system via similarity transformations. We employ homotopy analysis method (HAM) to construct analytic expressions of velocity, temperature and nanoparticles volume fraction. Convergence analysis is performed and optimal values of the convergence-control parameters are determined. The computations are validated with the built in routine for solving nonlinear boundary value problems via shooting technique through software Mathematica 8.0. The behaviors of key parameters such as suction/blowing parameter (A), squeeze parameter (S), Hartman number (M), Brownian motion parameter (Nb) and thermophoresis parameter (Nt) are thoroughly examined. It is seen that the parameters have a great impact on the concentration field for the suction flow when compared with the blowing case. An intensification in the Brownian motion and thermophoresis effects results in the appreciable increase in the temperature and nanoparticles concentration.

Keywords: squeezing flow, nanofluid, permeable disk, analytic solution, shooting method.

1 Introduction

Squeezing flows between parallel disks is an interesting topic of research because it occurs in many industrial applications which include polymer processing, compression, injection modeling, transient loading of mechanical components and the squeezed films in power transmission. The application of magnetic field in such flows allows us to prevent the unpredictable deviation of lubrication viscosity with temperature in certain extreme operating conditions. The seminal work on the topic under lubrication approximation has been studied by Stefan [1]. Theoretical analysis for squeezing flow of power-law fluid between parallel disks has been performed by Leider and Bird [2]. Domairry and

Aziz [3] provided the approximate analytic solution for the squeezing flow of viscous fluid between parallel disks with suction or blowing. Siddiqui et al. [4] discussed the effects of magnetic field in the squeezing flow between infinite parallel plates due to the normal motion of plates. Homotopy perturbation method (HPM) has been applied in [3,4] for the presentation of analytic solutions of the arising nonlinear problems. Two-dimensional and axisymmetric squeezing flows between parallel plates have been addressed by Rashidi et al. [5]. Joneidi et al. [6] provided the analytic and numerical solutions for magnetohydrodynamic squeezing flow between parallel disks. Squeezing flow of second grade fluid between parallel disks (one of which is porous) has been analyzed by Hayat et al. [7]. Heat transfer characteristics in the unidirectional squeezing flow between parallel disks have been studied by Duwairi et al. [8]. Mahmood et al. [9] obtained analytic solutions for squeezed flow and heat transfer over a porous plate. Local similarity method has been adopted to obtain the solution valid for all values of dimensionless time. However perturbation and asymptotic methods have been used to compute the solutions for small and large values of the dimensionless time. Khaled and Vafai [10] provided numerical solutions for hydromagnetic unsteady squeezing flow over a porous surface by a well established Thomas algorithm.

The term "nanofluid" refers to a liquid suspension containing tiny particles having diameter less than 100 nm. Choi [11] experimentally verified that addition of small amount of nanoparticles appreciably enhances the effective thermal conductivity of the base fluid. These particles are made up of the metals such as (Al, Cu), oxides (Al_2O3), carbides (SiC), nitrides (AlN, SiN) or nonmetals (graphite, carbon nanotubes). Buongiorno [12] proposed a mathematical model that considers two significant effects namely the Brownian motion and thermophoretic diffusion of nanoparticles. Kuznetsov and Nield [13] numerically studied the flow of nanofluid past a vertical flat plate. The Cheng–Minkowcz problem for natural convective boundary layer flow of a nanofluid occupying a porous space was considered by Nield and Kuznetsov [14]. Similar attempts in this direction include those of Nield and Kuznetsov [15,16] and Kuznetsov and Nield [17]. The boundary-layer flow of nanofluid over a continuously moving surface with a parallel free stream has been studied by Bachok et al. [18]. Khan and Pop [19] provided numerical solutions for boundary-layer flow of nanofluid over a stretching sheet. Hassani et al. [20] computed the analytic solutions for the problem considered in [19] by homotopy analysis method (HAM). Rana and Bhargava [21] numerically investigated the flow of nanofluid over a nonlinearly stretching sheet by finite element method (FEM). Makinde and Aziz [22] examined the flow of nanofluid over a stretching sheet in the presence of convective surface boundary conditions. Homotopy solutions for boundary layer stagnation-point flow of nanofluid towards a linearly stretching sheet have been obtained by Mustafa et al. [23]. Unsteady boundary layer flow of nanofluid over a stretching/shrinking sheet has been examined by Bachok et al. [24].

Existing information on the topic witnessed that squeezing flow of nanofluid has never been reported. This is first such study in the literature. The present paper looks at the time-dependent squeezing flow of nanofluid between two parallel disks where one is impermeable and the other is porous. The resulting mathematical problems have been solved by homotopy analysis method (HAM) proposed by Liao [25]. Based on the

homotopy of topology, HAM reduces the nonlinear differential equation to a set of linear ordinary differential equations which can be further solved by computational softwares such as Mathematica or Maple. This method distinguishes it self from other approximate numerical and analytical methods in a variety of ways. Unlike perturbative methods, HAM does not depend upon the existence of small/large parameters in the differential equations. In contrast to non-pertubative schemes HAM provides us a simple way to adjust and accelerate the convergence of the series solutions in the form of an auxiliary parameter $\hbar$. Moreover it can be efficiently employed to approximate strongly nonlinear problems by choosing different sets of base functions. The frequently used analytical tools namely the homotopy perturbation method (HPM), δ-expansion method and Adomian decomposition method (ADM) can be reduced as special cases of HAM. HAM has been recently applied to give analytic solutions of variety of nonlinear problems in science and engineering [26–31]. The expressions of skin friction coefficient, reduced Nusselt number and reduced Sherwood number are evaluated and discussed. The influences of embedding parameters on the flow fields are observed by plotting graphs.

2 Mathematical analysis

Consider the incompressible two-dimensional flow of nanofluid between parallel disks separated by a distance $h(t) = H(1 - at)^{1/2}$. A magnetic field of strength $B(t) = B_0(1 - at)^{-1/2}$ is applied perpendicular to the disks (see [7] for physical configuration and coordinate system). Here T_w and C_w denote the temperature and nanoparticles concentration at the lower disk while the temperature and concentration at the upper disk are T_h and C_h respectively. The upper disk at $z = h(t)$ moves towards or away from the stationary lower disk with the velocity $\mathrm{d}h/\mathrm{d}t$. The equations which governing the flow and mass transfer in viscous fluid are (see [13–24])

$$\frac{\partial u}{\partial r} + \frac{u}{r} + \frac{\partial w}{\partial z} = 0, \tag{1}$$

$$\frac{\partial u}{\partial t} + u\frac{\partial u}{\partial r} + w\frac{\partial u}{\partial z} = -\frac{1}{\rho_f}\frac{\partial \hat{p}}{\partial r} + \nu\left(\frac{\partial^2 u}{\partial r^2} + \frac{\partial^2 u}{\partial z^2} + \frac{1}{r}\frac{\partial u}{\partial r} - \frac{u}{r^2}\right), \tag{2}$$

$$\frac{\partial w}{\partial t} + u\frac{\partial w}{\partial r} + w\frac{\partial w}{\partial z} = -\frac{1}{\rho_f}\frac{\partial \hat{p}}{\partial z} + \nu\left(\frac{\partial^2 w}{\partial r^2} + \frac{\partial^2 w}{\partial z^2} + \frac{1}{r}\frac{\partial w}{\partial r}\right), \tag{3}$$

$$\begin{aligned}\frac{\partial T}{\partial t} &+ u\frac{\partial T}{\partial r} + w\frac{\partial T}{\partial z}\\ &= \alpha\left(\frac{\partial^2 T}{\partial r^2} + \frac{1}{r}\frac{\partial T}{\partial r} + \frac{\partial^2 T}{\partial z^2}\right)\\ &\quad + \tau\left[D_B\left(\frac{\partial C}{\partial r}\frac{\partial T}{\partial r} + \frac{\partial C}{\partial z}\frac{\partial T}{\partial z}\right) + \frac{D_T}{T_m}\left[\left(\frac{\partial T}{\partial r}\right)^2 + \left(\frac{\partial T}{\partial z}\right)^2\right]\right],\end{aligned} \tag{4}$$

$$\begin{aligned}\frac{\partial C}{\partial t} &+ u\frac{\partial C}{\partial r} + w\frac{\partial C}{\partial z}\\ &= D_B\left(\frac{\partial^2 C}{\partial r^2} + \frac{1}{r}\frac{\partial C}{\partial r} + \frac{\partial^2 C}{\partial z^2}\right) + \frac{D_T}{T_m}\left(\frac{\partial^2 T}{\partial r^2} + \frac{1}{r}\frac{\partial T}{\partial r} + \frac{\partial^2 T}{\partial z^2}\right).\end{aligned} \tag{5}$$

The boundary conditions are (see [3,6])

$$\begin{aligned} &u=0, \quad w=\frac{\mathrm{d}h}{\mathrm{d}t}, \quad T=T_h, \quad C=C_h && \text{at } z=h(t),\\ &u=0, \quad w=-\frac{w_0}{\sqrt{1-at}}, \quad T=T_w, \quad C=C_w && \text{at } z=0, \end{aligned}$$

where u and v are the velocity components in the r- and z-directions respectively, ρ is the density, μ is the dynamic viscosity, $\hat{p}$ is the pressure, T is the temperature, C is the nanoprticles concentration, α is the thermal diffusivity, D_B is the Brownian motion coefficient, D_T is the thermophoretic diffusion coefficient, T_m is the mean fluid temperature and k is the thermal conductivity. The last term in the energy equation is the total diffusion mass flux for nanoparticles, given as a sum of two diffusion terms (Brownian motion and thermophoresis) (please see [15] for derivation of last terms in Eqs. (4) and (5)). Further τ is the dimensionless parameter that gives the ratio of effective heat capacity of the nanoparticle material to heat capacity of the fluid. Thus value of τ will be, therefore, different for different fluids and nanoparticle materials. Using the following similarity transformations [3]

$$\begin{aligned} &u=\frac{ar}{2(1-at)}f'(\eta), \quad w=-\frac{aH}{\sqrt{1-at}}f(\eta), \quad \eta=\frac{z}{H\sqrt{1-at}},\\ &B(t)=\frac{B_0}{\sqrt{1-at}}, \quad \theta=\frac{T-T_h}{T_w-T_h}, \quad \phi=\frac{C-C_h}{C_w-C_h}, \end{aligned} \tag{6}$$

into Eqs. (2) and (3) and then eliminating the pressure gradient from the resulting equations we finally obtain

$$f''''-S\big(\eta f'''+3f''-2ff'''\big)-M^2f''=0. \tag{7}$$

Now Eqs. (4) and (5) take the following forms:

$$\theta''+PrS(2f\theta'-\eta\theta')+PrNb\,\theta'\phi'+PrNt\,\theta'^2=0, \tag{8}$$

$$\phi''+LeS(2f\phi'-\eta\phi')+\frac{Nt}{Nb}\theta''=0, \tag{9}$$

with the associated boundary conditions

$$\begin{aligned} &f(0)=A, \quad f'(0)=0, \quad \theta(0)=\phi(0)=1,\\ &f(1)=\frac{1}{2}, \quad f'(1)=0, \quad \theta(1)=\phi(1)=0, \end{aligned} \tag{10}$$

where S is the squeeze number, A is the suction/blowing parameter, M is the Hartman number, Nb is the Brownian motion parameter, Nt is the thermophoretic parameter, Pr is the Prandtl number and Le is the Lewis number which are defined as

$$\begin{aligned} &A=\frac{w_0}{aH}, \quad S=\frac{aH^2}{2\nu}, \quad M=\sqrt{\frac{\sigma B_0^2H^2}{\nu}}, \quad Pr=\frac{\nu}{\alpha}, \quad Le=\frac{\nu}{D_e},\\ &Nb=\frac{(\rho c)_pD_B(C_w-C_h)}{(\rho c)_f\nu}, \quad Nt=\frac{(\rho c)_pD_T(T_w-T_h)}{(\rho c)_fT_m\nu}. \end{aligned}$$

The continuity equation is identically satisfied. It is worth mentioning here that $A > 0$ indicates the suction of fluid from the lower disk while $A < 0$ represents injection flow. For $Nb = Nt = 0$, the problem reduces to the case of ordinary fluid (in which Brownian motion and thermophoretic effects are negligible). The physical quantities of interest are the skin friction coefficient C_{fr}, reduced Nusselt number Nur and reduced Sherwood number Shr which are defined by

$$C_{fr} = \frac{\tau_{rz}\big|_{z=h(t)}}{\rho(\frac{-aH}{2(1-at)^{1/2}})^2}, \quad Nu = \frac{Hq_w}{k(T_w - T_h)}, \quad Sh = \frac{Hj_w}{D_B(C_w - C_h)},$$

where

$$\tau_{rz} = \mu\left(\frac{\partial u}{\partial z} + \frac{\partial w}{\partial r}\right)\bigg|_{z=h(t)}, \quad q_w = -k\left(\frac{\partial T}{\partial z}\right)\bigg|_{z=h(t)}, \quad j_w = -D_B\left(\frac{\partial C}{\partial z}\right)\bigg|_{z=h(t)}.$$

In terms of variables (6) we have

$$\frac{H^2}{r^2}Re_r C_{fr} = f''(1), \quad Re_r = \frac{raH(1-at)^{1/2}}{2\nu},$$
$$Nur = (1-at)^{1/2}Nu = -\theta'(1), \quad Shr = (1-at)^{1/2}Sh = -\phi'(1).$$

3 Homotopy analytic solutions

Rule of solution expression and involved boundary conditions direct us to select the initial guesses and auxiliary linear operators as follows:

$$f_0(\eta) = (-1+2A)\eta^3 + \frac{1}{2}(3-6A)\eta^2 + A, \quad \theta_0(\eta) = \phi_0(\eta) = 1 - \eta,$$
$$\mathcal{L}_f \equiv \frac{\mathrm{d}^4}{\mathrm{d}\eta^4} - \frac{\mathrm{d}}{\mathrm{d}\eta}, \quad \mathcal{L}_\theta \equiv \frac{\mathrm{d}^2}{\mathrm{d}\eta^2}, \quad \mathcal{L}_\theta \equiv \frac{\mathrm{d}^2}{\mathrm{d}\eta^2}.$$

If $p \in [0,1]$ is an embedding parameter and $\hbar_1$ and $\hbar_2$ are the non-zero auxiliary parameters then the generalized homotopic equations corresponding to Eqs. (7)–(10) are

$$(1-p)\mathcal{L}_f\big[F(\eta,p) - F_0(\eta)\big] = p\hbar_1\mathcal{N}f\big[F(\eta,p)\big], \tag{11}$$
$$(1-p)\mathcal{L}_\theta\big[\Theta(\eta,p) - \Theta_0(\eta)\big] = p\hbar_2\mathcal{N}_\theta\big[F(\eta,p),\Theta(\eta,p),\Phi(\eta,p)\big], \tag{12}$$
$$(1-p)\mathcal{L}_\phi\big[\Phi(\eta,p) - \Phi_0(\eta)\big] = p\hbar_2\mathcal{N}_\phi\big[F(\eta,p),\Theta(\eta,p),\Phi(\eta,p)\big], \tag{13}$$

$$F(0,p) = A, \quad \frac{\partial F}{\partial \eta}\bigg|_{\eta=0} = 0, \quad \Theta(0,p) = 0, \quad \Phi(0,p) = 0, \tag{14}$$

$$\frac{\partial F}{\partial \eta}\bigg|_{\eta=1} = 0, \quad \Theta(1,p) = \Phi(1,p) = 0, \tag{15}$$

$$\begin{aligned}
&\mathcal{N}_f\big[F(\eta,p)\big]\\
&\quad=\frac{\partial^4 F(\eta,p)}{\partial\eta^4}-S\bigg(\eta\frac{\partial^3 F(\eta,p)}{\partial\eta^3}+3\frac{\partial^2 F(\eta,p)}{\partial\eta^2}-2F(\eta,p)\frac{\partial^3 F(\eta,p)}{\partial\eta^3}\bigg)\\
&\qquad-M^2\frac{\partial^2 F(\eta,p)}{\partial\eta^2},\\
&\mathcal{N}_\theta\big[F(\eta,p),\Theta(\eta,p),\Phi(\eta,p)\big]\\
&\quad=\frac{\partial^2\Theta(\eta,p)}{\partial\eta^2}+SPr\bigg(2F(\eta,p)\frac{\partial\Theta(\eta,p)}{\partial\eta}-\eta\frac{\partial\Theta(\eta,p)}{\partial\eta}\bigg)\\
&\qquad+PrNb\frac{\partial\Theta(\eta,p)}{\partial\eta}\frac{\partial\Phi(\eta,p)}{\partial\eta}+PrNt\bigg(\frac{\partial\Theta(\eta,p)}{\partial\eta}\bigg)^2,\\
&\mathcal{N}_\phi\big[F(\eta,p),\Theta(\eta,p),\Phi(\eta,p)\big]\\
&\quad=\frac{\partial^2\Phi(\eta,p)}{\partial\eta^2}+SLe\bigg(2F(\eta,p)\frac{\partial\Phi(\eta,p)}{\partial\eta}-\eta\frac{\partial\Phi(\eta,p)}{\partial\eta}\bigg)+\frac{Nt}{Nb}\frac{\partial^2\Theta(\eta,p)}{\partial\eta^2}.
\end{aligned}$$

Expanding F, Θ and Φ using the Maclaurin's series about p we get

$$F(\eta,p)=\sum_{m=0}^{\infty}f_m(\eta)p^m,\quad f_m(\eta)=\frac{1}{m!}\frac{\partial^m F(\eta,p)}{\partial p^m}\Big|_{p=0},\tag{16}$$

$$\Theta(\eta,p)=\sum_{m=0}^{\infty}\theta_m(\eta)p^m,\quad \theta_m(\eta)=\frac{1}{m!}\frac{\partial^m \Theta(\eta,p)}{\partial p^m}\Big|_{p=0},\tag{17}$$

$$\Phi(\eta,p)=\sum_{m=0}^{\infty}\phi_m(\eta)p^m,\quad \phi_m(\eta)=\frac{1}{m!}\frac{\partial^m \Phi(\eta,p)}{\partial p^m}\Big|_{p=0},\tag{18}$$

and the final solutions can be retrieved at $p=1$. The functions f_m, g_m and θ_m can be obtained through the deformation of Eqs. (11)–(15). Explicit mth-order deformation equations corresponding to the problems (11)–(15) are

$$\begin{aligned}
\mathcal{L}_f\big[f_m(\eta)-\chi_m f_{m-1}(\eta)\big]&=\hbar_1\mathcal{R}_m^f(\eta),\\
\mathcal{L}_\theta\big[\theta_m(\eta)-\chi_m\theta_{m-1}(\eta)\big]&=\hbar_2\mathcal{R}_m^\theta(\eta),\\
\mathcal{L}_\phi\big[\phi_m(\eta)-\chi_m\phi_{m-1}(\eta)\big]&=\hbar_2\mathcal{R}_m^\phi(\eta),
\end{aligned}$$

$$\begin{aligned}
&f_m(0)=0,\quad f_m'(0)=0,\quad \theta_m(0)=0,\quad \phi_m(0)=0,\\
&f_m(1)=0,\quad f_m'(1)=0,\quad \theta_m(1)=0,\quad \phi_m(1)=0,
\end{aligned}$$

$$\begin{aligned}
\mathcal{R}_m^f(\eta)&=f_{m-1}''''-S\big(\eta f_{m-1}'''+3f_{m-1}''\big)-M^2f_{m-1}''+2S\sum_{k=0}^{m-1}f_{m-1-k}f_k''',\\
\mathcal{R}_m^\theta(\eta)&=\theta_{m-1}''-SPr\eta\theta_{m-1}'+PrNb\sum_{k=0}^{m-1}\theta_{m-1-k}'\phi_k'+2SPr\sum_{k=0}^{m-1}f_{m-1-k}\theta_k'\\
&\quad+PrNt\sum_{k=0}^{m-1}\theta_{m-1-k}'\theta_k',
\end{aligned}$$

$$\mathcal{R}_m^{\phi}(\eta) = \phi''_{m-1} - SLe\,\eta\phi'_{m-1} + \frac{Nt}{Nb}\phi''_{m-1} + 2SLe\sum_{k=0}^{m-1} f_{m-1-k}\phi'_k,$$

$$\chi_m = \begin{cases} 0, & m = 1, \\ 1, & m > 1. \end{cases}$$

4 Error analysis and selection of optimal values of convergence-control parameters

It is clear that Eqs. (16)–(18) contain the so called auxiliary parameters $\hbar_1$ and $\hbar_2$. As pointed out by Liao [25], the convergence of the series solutions is highly dependent on the choice of these parameters. To determine the optimal values of these parameters we define the averaged residuals errors for the functions f, θ and ϕ as

$$E_{m,1}(\hbar_1) = \frac{1}{K}\sum_{i=0}^{K}\left[\mathcal{N}_f\left(\sum_{j=0}^{m} f_j(i\Delta x)\right)\right]^2, \tag{19}$$

$$E_{m,2}(\hbar_2) = \frac{1}{K}\sum_{i=0}^{K}\left[\mathcal{N}_\theta\left(\sum_{j=0}^{m} \theta_j(i\Delta x), \sum_{j=0}^{m} \phi_j(i\Delta x)\right)\right]^2, \tag{20}$$

$$E_{m,2}(\hbar_2) = \frac{1}{K}\sum_{i=0}^{K}\left[\mathcal{N}_\phi\left(\sum_{j=0}^{m} \theta_j(i\Delta x), \sum_{j=0}^{m} \phi_j(i\Delta x)\right)\right]^2, \tag{21}$$

where $\Delta x = 1/K$ and $K = 20$. The above averaged residual errors can be plotted versus the respective auxiliary parameters to determine the convergence region of the solutions. For a given order of approximations m, the optimal values of $\hbar_1$ and $\hbar_2$ can be determined by minimizing the averaged residual error given in Eqs. (19)–(21) using the command *Minimize* of the software Mathematica 8.0. In Tables 1 and 2, the optimal values of $\hbar_1$ and $\hbar_2$ for the functions f, θ and ϕ corresponding to various values of the parameters are given. Here the corresponding averaged residuals are represented as $E^*_{m,1}$, $E^*_{m,2}$ and

Table 1. Optimal values of $\hbar_1$ for different values of the parameters.

M	S	$A = 2$		$A = -2$	
		Optimal value of $\hbar_1$	$E^*_{m,1}$	Optimal value of $\hbar_1$	$E^*_{m,1}$
0	1	-0.868	3.06×10^{-14}	-0.889	8.32×10^{-12}
2		-0.855	2.23×10^{-15}	-0.833	1.00×10^{-12}
3		-0.856	1.21×10^{-15}	-0.772	9.18×10^{-14}
5		-0.791	1.04×10^{-11}	-0.720	1.64×10^{-11}
1	1/10	-0.904	8.97×10^{-24}	-0.868	6.16×10^{-24}
	1/2	-0.916	3.38×10^{-22}	-0.906	1.05×10^{-20}
	1	-0.862	1.68×10^{-14}	-0.874	4.92×10^{-12}
	2	-0.753	1.75×10^{-6}	-0.906	1.05×10^{-20}

$E^*_{m,3}$ respectively. For a further check at the accuracy of our computations we compared HAM solutions with the numerical solutions obtained through the command *NDSolve* of the software Mathematica 8.0. The results are in excellent agreement as can be seen from Tables 3 and 4.

Table 2. Optimal values of $\hbar_2$ for different values of the parameters when $M = S = 1$, $A = 2$ and $\hbar_1 = -0.862$.

Nb	Nt	Optimal value of $\hbar_2$ for θ	$E^*_{m,2}$	Optimal value of $\hbar_2$ for ϕ	$E^*_{m,3}$
$1/10$	$1/10$	-0.908	1.47×10^{-11}	-0.936	2.51×10^{-10}
$1/2$		-0.915	1.62×10^{-13}	-0.941	1.18×10^{-12}
1		-0.931	9.10×10^{-13}	-0.894	4.11×10^{-13}
$3/2$		-0.921	4.51×10^{-12}	-0.886	2.86×10^{-13}
	$1/2$	-0.961	2.93×10^{-10}	-0.913	2.87×10^{-10}
	1	-1.021	1.21×10^{-8}	-0.953	2.97×10^{-8}
	$3/2$	-0.955	2.37×10^{-6}	-1.027	1.18×10^{-5}
	2	-0.820	1.00×10^{-4}	-0.916	4.21×10^{-4}

Table 3. Values of skin friction coefficient $f''(1)$ for different values of M and S.

M	S	$f''(1)$	
		HAM	NDSolve
0	1	7.53316579	7.53316579
2		8.26387231	8.26387230
3		9.09732572	9.09732573
5		11.3492890	11.3492890
1	$1/10$	8.97552394	8.97552394
	$1/2$	8.34924578	8.34924578
	1	7.72194601	7.72194601
	2	6.94077326	6.94077334

Table 4. Values of reduced Nusselt number Nur and reduced Sherwood number Shr for different values of Nb and Nt when $A = 2$, $M = S = Pr = Le = 1$ and $\hbar_1 = -0.862$.

Nb	Nt	Nur		Shr	
		HAM	NDSolve	HAM	NDSolve
$1/10$	$1/10$	0.52628540	0.52628539	0.86604666	0.86604666
$1/2$		0.63433253	0.63433253	0.53012814	0.53012814
1		0.78636385	0.78636384	0.48603919	0.48603919
$3/2$		0.95569955	0.95569954	0.46986157	0.46986157
	$1/2$	1.17682119	1.17682119	0.40180718	0.40180718
	1	1.48581207	1.48581194	0.12619334	0.12619330
	$3/2$	1.82305276	1.82305354	0.39083080	0.39083988
	2	2.17915991	2.17922795	1.16777723	1.16800856

5 Numerical results and discussion

Representative results for velocity, temperature and nanoparticles concentration have been presented graphically and in tabular form. The values of $S > 0$ corresponds to the upward motion of disk while $S < 0$ indicates that upper disk is moving towards the stationary lower disk. It is also clear that an increase in S may be either regarded as an increase in the velocity of the upper disk or the distance between the disks. It is clear from Fig. 1 that velocity decreases initially with an increase in S in the blowing case, however when η reaches the neighborhood of 0.55 it starts increasing by increasing S. The behavior of squeeze parameter S for suction flow is opposite to that accounted for the blowing case. In the case of suction ($A > 0$), the maxima in the profiles is shifted towards the upper disk when S is increased. However the profiles are tilted towards the lower disk when S is increased in the blowing case ($A < 0$). Fig. 2 plots the effect of Hartman number M on velocity f'. The Hartman number M which describes the strength of Lorentz force due to magnetic field can take any value in the interval $[0, \infty]$. For $M = 0$ the governing equations for the hydrodynamic flow are recovered. The velocity increases initially with an increase in S. Since the same mass flow rate is imposed, in order to satisfy the mass conservation constraint, with increased M we would expect that the increase in the fluid velocity in the wall regions will be compensated by a decrease in the fluid velocity near the central region giving rise to a cross-flow behavior.

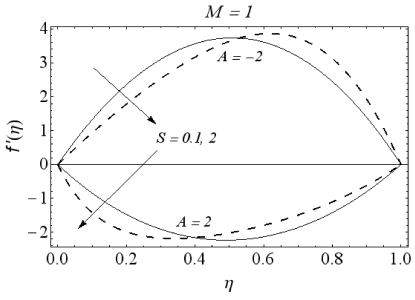

Fig. 1. Influence of S on $f'(\eta)$.

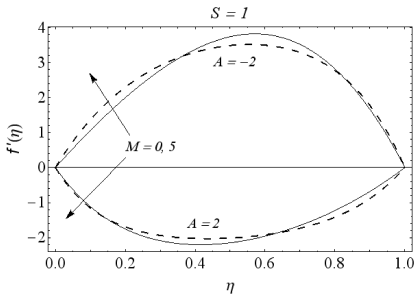

Fig. 2. Influence of M on $f'(\eta)$.

The effects of Brownian motion and thermophoresis parameters Nb and Nt on the temperature field θ are discussed in the Figs. 3 and 4. Here the solid lines indicate the profiles for suction flow ($A > 0$) whereas the profiles in the blowing case ($A < 0$) are represented by dashed lines. It is seen that θ decreases monotonically from $\eta = 0$ to $\eta = 1$. It is important to note that parameters Nb and Nt characterize the strengths of Brownian motion and thermophoresis effects. The larger the values of Nb and Nt, the greater will be the strength of the corresponding effects. Thus Nb and Nt can take any value in the range $0 \leq Nb$, $Nt < \infty$. It is worth pointing here that the liquid metals are characterize by small values of Pr ($\ll 1$), which have high thermal conductivity but low viscosity, while large values of Pr ($\gg 1$) correspond to high-viscosity oils. Specifically, Prandtl number $Pr = 0.72$, 1.0 and 7.0 correspond to air, electrolyte solution such as salt water and water, respectively [32]. In our computations we have chosen $Pr = 1$ to

retrieve all the graphical results. The temperature θ significantly rises and profiles move closer to the upper disk as Nb and Nt increase in both the suction and blowing cases. This results in the larger rate of heat transfer at the upper disk (as evident from Table 2). The influence of these parameters on the nanoparticles volume fraction ϕ is illustrated in the Figs. 5 and 6. An increase in Nb effectively increases the nanoparticles concentration. This increase is due to the effective movement of nanoparticles from the upper disk to the fluid. It is interesting to see that the deviation in the profiles only occur for the values of Nb in the range $0 \leq Nb \leq 2$. However nanopaticles concentration is negligibly affected for the values of Nb beyond 2.0. There is an appreciable increase in the concentration function ϕ as the thermophoretic effect intensifies. From the physical point of view an increase in the thermophoretic effect generates the larger mass flux due to temperature gradient which in turn rises the concentration.

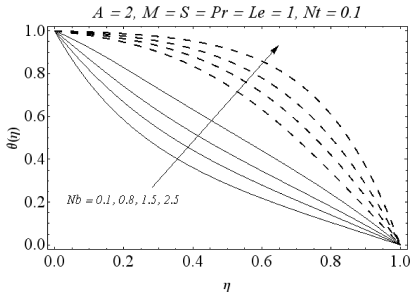

Fig. 3. Influence of Nb on $\theta(\eta)$.

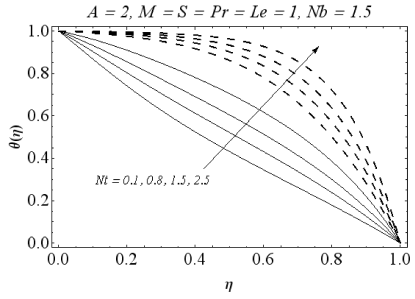

Fig. 4. Influence of Nt on $\theta(\eta)$.

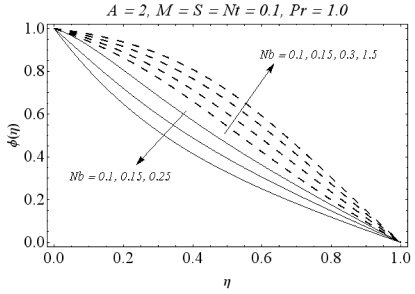

Fig. 5. Influence of Nb on $\phi(\eta)$.

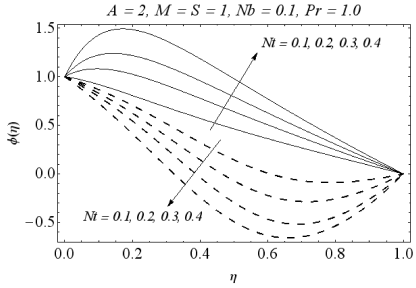

Fig. 6. Influence of Nt on $\phi(\eta)$.

The combined influence of Brownian motion and thermophoresis parameters on the reduced Nusselt and Sherwood numbers is depicted from Figs. 7 and 8. We notice that for a weaker thermophoretic diffusion there is a slight increase in the magnitude of Nur with an increase in Nb. However this increase is more pronounced for sufficiently stronger thermophoretic effect. Further we found a significant increase in the reduced Sherwood number when Nb and Nt are increased. There is hardly any change in Shr for sufficiently large values of Nb. Tables 3 provides the numerical values of skin friction coefficient for different values of embedding parameters. For fixed values of S and M, an increase in the

suction/blowing velocity corresponds to a larger rate of stress at the upper disk. However larger values of A indicates smaller mass transfer rate from the disk. The magnitude of skin friction coefficient gradually decreases as the disk moves in the upward direction. Further it is seen that an increase in the magnetic field strength increases the magnitude of skin friction coefficient. In Table 4 the numerical values of reduced Nusselt number and reduced Sherwood number have been tabulated for different values of Nb and Nt. Tables 3 and 4 also indicate that HAM solutions agrees very well with the numerical solutions for all the values of the parameters.

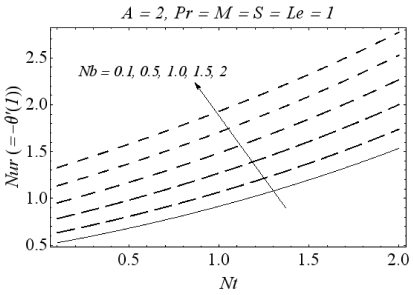

Fig. 7. Influence of Nb and Nt on Nur.

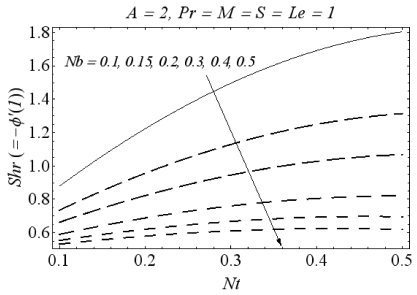

Fig. 8. Influence of Nb and Nt on Shr.

6 Conclusions

Magnetohydrodynamic (MHD) squeezing flow of nanofluid between parallel disks is studied. The modeled differential equations are solved by homotopy analysis method (HAM). A very good averaged residual error is obtained at only 15th-order homotopy solutions. Moreover homotopy solutions are found in excellent agreement with the numerical solutions. The results indicate an increase in the skin friction coefficient with an increase in the strength of magnetic field. From the industrial point of view this outcome is undesirable since the drag force in squeezing the fluid between the disks increases as the magnetic field strength increases. We found that temperature θ appreciably rises when Nb and Nt are increased for some fixed values of other parameters. This increase accompanies with the increasingly steeper profiles which indicate an augmentation in the rate of heat transfer at the upper disk. On the other hand the nanoparticles volume fraction at the disk decreases with an intensification in the Brownian motion effect. The behaviors of parameters on the temperature are similar in both suction and injection cases. However opposite trend is noticed for the nanoparticles volume fraction. The current analysis for the case of ordinary fluid can be recovered from the presented series solutions when $Nb = Nt = 0$.

Acknowledgement

We warmly thank the learned reviewer for his constructive and useful suggestions. The research of Dr. Alsaedi was partially supported by Deanship of Scientific Research (DSR), King Abdulaziz University, Jeddah, Saudi Arabia.

References

1. M.J. Stefan, Versuch Über die scheinbare Adhäsion, *Sitzungsber., Abt. II, Österr. Akad. Wiss., Math.-Naturwiss. Kl.*, **69**, pp. 713–721, 1874.

2. P.J. Leider, R.B. Bird, Squeezing flow between parallel disks. I. Theoretical analysis, Ind. Eng. Chem. Fundam., **13**, pp. 336–341, 1974.

3. G. Domairry, A. Aziz, Approximate analysis of MHD Squeeze flow between two parallel disks with suction or injection by homotopy perturbation method, *Math. Probl. Eng.*, doi: 10.1155/2009/603916.

4. A.M. Siddiqui, S. Irum, A.R. Ansari, Unsteady squeezing flow of a viscous MHD fluid between parallel plates, *Math. Model. Anal.*, **13**, pp. 565–576, 2008.

5. M.M. Rashidi, H. Shahmohamadi,S. Dinarvand, Analytic approximate solutions for unsteady two-dimensional and axisymmetric squeezing flows between parallel plates, *Math. Probl. Eng.*, doi: 10.1155/2008/935095.

6. A.A. Joneidi, G. Domairry, M. Babaelahi, Effect of mass transfer on the flow in the magnetohydrodynamic squeeze film between two parallel disks with one porous disk, *Chem. Eng. Commum.*, **198**, pp. 299–311, 2011.

7. T. Hayat, A. Yousaf, M. Mustafa, S. Obaidat, MHD squeezing flow of second-grade fluid between two parallel disks, *Int. J. Numer. Methods Fluids*, doi: 10.1002/fld.2565.

8. H.M. Duwairi, B. Tashtoush, R.A. Domseh, On heat transfer effects of a viscous fluid squeezed and extruded between two parallel plates, *Heat Mass Transfer*, **14**, pp. 112–117, 2004.

9. M. Mahmood, S. Asghar, M.A. Hossain, Squeezed flow and heat transfer over a porous surface for viscous fluid, *Heat Mass Transfer*, **44**, pp. 165–173, 2007.

10. A.R.A. Khaled, K. Vafai, Hydromagnetic squeezed flow and heat transfer over a sensor surface, *Int. J. Eng. Sci.*, **42**, pp. 509–519, 2004.

11. S.U.S. Choi, Enhancing thermal conductivity of fluids with nanoparticle, in: D.A. Siginer, H.P. Wang (Eds.), *Developments and Applications of Non-Newtonian Flows*, Vol. FED 231, ASME, New York, 1995, pp. 99–105.

12. J. Buongiorno, Convective transport in nanofluids, *J. Heat Transfer*, **128**, pp. 240–250, 2006.

13. A.V. Kuznetsov, D.A. Nield, Natural convective boundary-layer flow of a nanofluid past a vertical plate, *Int. J. Therm. Sci.*, **49**, pp. 243–247, 2010.

14. D.A. Nield, A.V. Kuznetsov, The Cheng–Minkowycz problem for natural convective boundary-layer flow in a porous medium saturated by a nanofluid, *Int. J. Heat Mass Transfer*, **52**, pp. 5792–5795, 2009.

15. D.A. Nield, A.V. Kuznetsov, The onset of convection in a horizontal nanofluid layer of finite depth, *Eur. J. Mech., B, Fluids*, **29**, pp. 217–223, 2010.

16. D.A. Nield, A.V. Kuznetsov, The Cheng–Minkowycz problem for the double-diffusive natural convective boundary layer flow in a porous medium saturated by a nanofluid, *Int. J. Heat Mass Transfer*, **54**, pp. 374–378, 2011.

17. A.V. Kuznetsov, D.A. Nield, Double-diffusive natural convective boundary-layer flow of a nanofluid past a vertical plate, *Int. J. Therm. Sci.*, **50**, pp. 712–717, 2011.

18. N. Bachok, A. Ishak, I. Pop, Boundary-layer flow of nanofluids over a moving surface in a flowing fluid, *Int. J. Therm. Sci.*, **49**, pp. 1663–1668, 2010.

19. W.A. Khan, I. Pop, Boundary-layer flow of a nanofluid past a stretching sheet, *Int. J. Heat Mass Transfer*, **53**, pp. 2477–2483, 2010.

20. M. Hassani, M.M. Tabar, H. Nemati, G. Domairry, F. Noori, An analytical solution for boundary layer flow of a nanofluid past a stretching sheet, *Int. J. Therm. Sci.*, **50**, pp. 2256–2263, 2011.

21. P. Rana, R. Bhargava, Flow and heat transfer of a nanofluid over a nonlinearly stretching sheet: A numerical study, *Commun. Nonlinear Sci. Numer. Simul.*, doi: 10.1016/j.cnsns.2011.05.009.

22. O. Makinde, A. Aziz, Boundary layer flow of a nanofluid past a stretching sheet with a convective boundary condition, *Int. J. Therm. Sci.*, **50**, pp. 1326–1332, 2011.

23. M. Mustafa, T. Hayat, I. Pop, S. Asghar, S. Obaidat, Stagnation-point flow of a nanofluid towards a stretching sheet, *Int. J. Heat Mass Transfer*, **54**, pp. 5588–5594, 2011.

24. N. Bachok, A. Ishak, I. Pop, Unsteady boundary-layer flow and heat transfer of a nanofluid over a permeable stretching/shrinking sheet, *Int. J. Heat Mass Transfer*, **55**, pp. 2102–2109, 2012.

25. S.J. Liao, Notes on the homotopy analysis method: Some definitions and theorems, *Commun. Nonlinear Sci. Numer. Simul.*, **14**, pp. 983–997, 2009.

26. S.J. Liao, On the relationship between the homotopy analysis method and Euler transform, *Commun. Nonlinear Sci. Numer. Simul.*, **15**, pp. 1421–1431, 2010.

27. S. Abbasbandy, E. Shivanian, K. Vajravelu, Mathematical properties of $\hbar$-curve in the frame work of the homotopy analysis method, *Commun. Nonlinear Sci. Numer. Simul.*, **16**, pp. 4268–4275, 2011.

28. S. Abbasbandy, Homotopy analysis method for the Kawahara equation, *Nonlinear Anal., Real World Appl.*, **11**, pp. 307–312, 2010.

29. M.M. Rashidi, S.A.M. Pour, S. Abbasbandy, Analytic approximate solutions for heat transfer of a micropolar fluid through a porous medium with radiation, *Commun. Nonlinear Sci. Numer. Simul.*, **16**, pp. 1874–1889, 2011.

30. T. Hayat, M. Mustafa, S. Asghar, Unsteady flow with heat and mass transfer of a third grade fluid over a stretching surface in the presence of chemical reaction, *Nonlinear Anal., Real World Appl.*, **11**, pp. 3186–3197, 2010.

31. M. Mustafa, T. Hayat, I. Pop, S. Obaidat, Stagnation-point flow and heat transfer of a Casson fluid towards a stretching sheet, *Z. Naturforsch., A*, **67**, pp. 70–76, 2012.

32. M.Z. Salleh, R. Nazar, I. Pop, Boundary layerflow and heat transfer over a stretching sheet with Newtonian heating, *J. Taiwan Inst. Chem. Eng.*, **41**, pp. 651–655, 2010.